Geophysical Journal International

Geophys. J. Int. (2010) doi: 10.1111/j.1365-246X.2010.04640.x

Twentieth century constraints on sea level change and earthquake deformation at Macquarie Island

Christopher Watson,[1,4] Reed Burgette,[1] Paul Tregoning,[2] Neil White,[3] John Hunter,[4] Richard Coleman,[5,4] Roger Handsworth[6] and Henk Brolsma[6]

[1] *Surveying and Spatial Science Group, School of Geography and Environmental Studies, University of Tasmania, Private Bag* 76, *Hobart, Tasmania* 7001, *Australia. E-mail: cwatson@utas.edu.au*

[2] *Research School of Earth Sciences, The Australian National University, Canberra, ACT, Australia*

[3] *Centre for Australian Weather and Climate Research, A Partnership Between CSIRO and the Australian Bureau of Meteorology, CSIRO Marine and Atmospheric Research, GPO Box* 1538, *Hobart, Tasmania* 7001, *Australia*

[4] *Antarctic Climate and Ecosystems Cooperative Research Centre, University of Tasmania, Private Bag* 80, *Hobart, Tasmania* 7001, *Australia*

[5] *Institute for Marine and Antarctic Studies, University of Tasmania, Private Bag* 78, *Hobart, Tasmania* 7001, *Australia*

[6] *Australian Antarctic Division, Channel Highway, Kingston, Tasmania* 7050, *Australia*

Accepted 2010 April 26. Received 2010 April 20; in original form 2009 November 24

SUMMARY

Through the combination of rare historical sea level observations collected during Sir Douglas Mawson's 1911–1914 Australasian Antarctic Expedition (AAE), together with modern sea level data, space geodetic estimates of crustal displacement and modelling of coseismic and post-seismic earthquake deformation, we present a contemporary analysis to constrain sea level and land level change over the twentieth century at Macquarie Island (54°30′S, 158°57′E). We combine 9 months of 1912–1913 sea level data with intermediate observations in 1969–1971, 1982 and 1998–2007 to estimate sea level rise relative to the land at +4.8 ± 0.6 mm yr^{-1}. Combined with estimates of global mean sea level rise, this value supports the geologically surprising notion of land subsidence, conflicting with longer term geological evidence that suggests uplift at ∼0.8 mm yr^{-1} over the last 400–300 Kyr. We investigate the current tectonic evolution of the Island through analysis of Global Positioning System (GPS) solutions that utilize data over the period 2000–2009. Importantly, this provides an opportunity to refine the source parameters of the M_w ∼8.0 great earthquake of 2004 December 23 using estimates of coseismic displacements at regional GPS sites. We use the estimated earthquake source and GPS observations of four years of post-seismic deformation at Macquarie Island to infer the rheology of the oceanic upper mantle. We find that an asthenosphere bounded by stronger material above and below is required to produce the observed post-seismic deformation, particularly in the vertical component. Assuming a Maxwell rheology, the best fit is given by an asthenospheric viscosity of 3×10^{19} Pa s. The inferred rheology determined from the 2004 earthquake is used to model long period post-seismic deformation from M_w ∼8.0 earthquakes of 1989 and 1924. The 1924 earthquake is the closest of the three great earthquakes to Macquarie Island, and our modelling suggests that the majority of the vertical deformation at the tide gauge over the subsequent 80 years is related to ongoing viscoelastic relaxation from this thrust earthquake that ruptured south from an epicentre south of Macquarie Island. Assimilated time-series of land level change from the earthquake modelling (suggesting ongoing subsidence) constrained by the GPS estimate of vertical velocity of −2.46 ± 0.64 mm yr^{-1} combine with the relative sea level time-series to yield an estimate of absolute sea level change of +2.0 ± 0.8 mm yr^{-1} over the twentieth century. We conclude this is consistent with the upper bound of the global average rate of absolute sea level rise over the same period. This represents one of few estimates of observed sea level change in the Southern Ocean, re-emphasizing the importance of historical data and continued geodetic and oceanographic observation in remote areas.

Key words: Sea level change; Space geodetic surveys; Seismic cycle; Transient deformation; Oceanic transform and fracture zone processes; Rheology: mantle.

1 INTRODUCTION AND METHODOLOGY

Global average sea level rise has been estimated to be $+1.7 \pm 0.5$ mm yr^{-1} over the twentieth century (Bindoff *et al.* 2007). This estimate is largely constrained by a small set of long running tide gauges that show a highly irregular distribution and bias towards the northern hemisphere (Emery & Aubrey 1991). The geographic distribution of tide gauge sites archived by the Permanent Service for Mean Sea Level (PSMSL; Woodworth & Player 2003) emphasizes the conspicuous paucity of data south of the equator and specifically in and around the Southern Ocean. The void of long-term sea level measurements throughout the Southern Ocean has the potential to bias estimates of both global and regional sea level change, including those derived using reconstruction techniques that utilize modern satellite altimetry and/or sparse historic tide gauge data (e.g. Church *et al.* 2004; Jevrejeva *et al.* 2006).

In an attempt to provide further insight into sea level change in data sparse regions, various studies have investigated historical tide gauge records. Notable examples include sites at Port Arthur (Hunter *et al.* 2003), Liverpool (Woodworth, 1999), Brest (Wöppelmann *et al.* 2006), Kergeulen Island (Testut *et al.* 2006) and Key West (Maul & Martin 1993). Current work is also underway at Commonwealth Bay, Antarctica (L. Testut, personal communication, 2009) and on the Falkland Islands (Woodworth *et al.* 2010). Common to all 'data archaeology' investigations is the analysis of historic sea level that is connected via a common datum to more recent or modern-day estimates of sea level enabling the estimation of change over comparatively long timescales.

Meaningful estimates of absolute sea level change from such historical studies are often limited by highly uncertain estimates of vertical motion of the crust at the gauge location. In this study, we base our investigation on data observed at Macquarie Island (54°30′S, 158°57′E) during Sir Douglas Mawson's 1911–1914 Australasian Antarctic Expedition (AAE). The Island itself is the culmination of a bathymetric ridge along the Australia–Pacific Plate boundary known as the Macquarie Ridge Complex (MRC). The MRC region has been the location of numerous historical earthquakes, including two of the largest transform earthquakes in the instrumental record; the M_w 8.0–8.1 earthquakes of 1989 and 2004 (Fig. 1). Estimates of vertical deformation from regional earthquakes at the tide gauge are crucial for understanding the absolute sea level change component of the observed relative sea level record.

This paper provides a contemporary constraint on both present-day sea level and land level change by coupling historical and modern sea level records, space geodetic estimates of crustal motion and modelling of coseismic and post-seismic earthquake deformation that may have affected tide gauge estimates of sea level. In Section 2, we employ simple harmonic tidal analyses to estimate local mean sea level (MSL) for annual (or near annual) bins of data over time. Each estimate of MSL is linked to the same datum using connections derived between tide gauges and permanent tide gauge benchmarks (BMs). Uncertainty bounds on estimates of MSL are derived using satellite altimeter data as a proxy to determine the magnitude of inter-annual variability in this region of the Southern Ocean. In Section 3, we combine the various estimates of MSL with their uncertainties to estimate relative sea level change over a ∼100 yr period. In Section 4, we investigate the land motion using analysis of Global Positioning System (GPS) data that includes the Macquarie Island GPS site 'MAC1' from the International Global Navigation Satellite Systems Service (IGS, Dow *et al.* 2005), solving for both vertical rates of motion as well as coseismic and post-seismic deformations. We used simple modelling of regional coseismic deformation from the recent great M_w 8.1 event (2004.9771) to better resolve the source parameters of the earthquake. We used these estimated coseismic parameters as the input for a simplified model of post-seismic deformation, using the observed post-seismic deformation from the MAC1 GPS site to constrain a plausible upper mantle rheology structure. Finally, we used the available seismological constraints on past major earthquakes to place bounds on the vertical deformation that occurred at the tide gauge site from earthquakes that preceded the geodetic record. In Section 5, we combine these data to yield a constraint on the rate of absolute sea level rise and land level change at this remote and important geodetic and oceanographic observing station.

2 SEA LEVEL DATA AND DATUM CONTROL

2.1 Historic sea level data

Nine months of sea level data were obtained on Macquarie Island using an automatic float gauge between 1912 August and 1913 May (locality shown in Fig. 2). Data from this period were first analysed by Doodson (1939), who also documented important datum information which has been critical for this study. Copies of the original tide gauge charts obtained from the Mitchell Library (Sydney, Australia) were digitized by the Australian National Tidal Centre and subsequently analysed using a modern harmonic approach as part of this investigation. Utilizing T_Tide analysis software (V1.2; Pawlowicz *et al.* 2002), the modern estimation of MSL over this period agrees with that computed by Doodson (1939) to within the number of significant digits reported (equating to <3 mm). The tidal data appears to be of high quality, with the non-tidal residuals having a standard deviation of 0.14 m.

Various unsuccessful attempts were made to observe sea level in the years since the Australian National Antarctic Research Expeditions (ANARE) established a permanent station on Macquarie Island in 1948. Valuable data have been extracted between 1969 March and 1971 January (McCue 1971), observed using an automatic float gauge in an area adjacent to the site of the Australasian Antarctic Expedition (AAE) installation (Fig. 2). Other data observed in 1964, 1967–1968, 1972–1974 have been obtained but are of little use given equipment malfunction or lack of appropriate datum information. The 1969–1971 data were successfully connected by levelling to the AAE BM and are of high quality with comparable non-tidal variability (0.13 m) to that observed previously. A total of 12 days of observations were also obtained in 1982 January using an Aanderaa pressure gauge (Corcoran 1982). Given the large uncertainty associated with this very short record, the MSL estimate determined from the 1982 data has been incorporated into this study for comparative purposes only.

2.2 Modern sea level data

The modern era of tidal observations began with an Aquatrak acoustic gauge installed in 1993 December (Fig. 2). Given unique aspects of the installation (inclined orientation and custom stilling well and orifice), specific effort has been placed on calibration to solve for range-dependent and draw-down effects (Watson *et al.* 2008). As part of the calibration study, Watson *et al.* (2008) used four independent GPS buoy deployments to compute offset, scale and sea state dependent draw-down parameters for the acoustic gauge, enabling

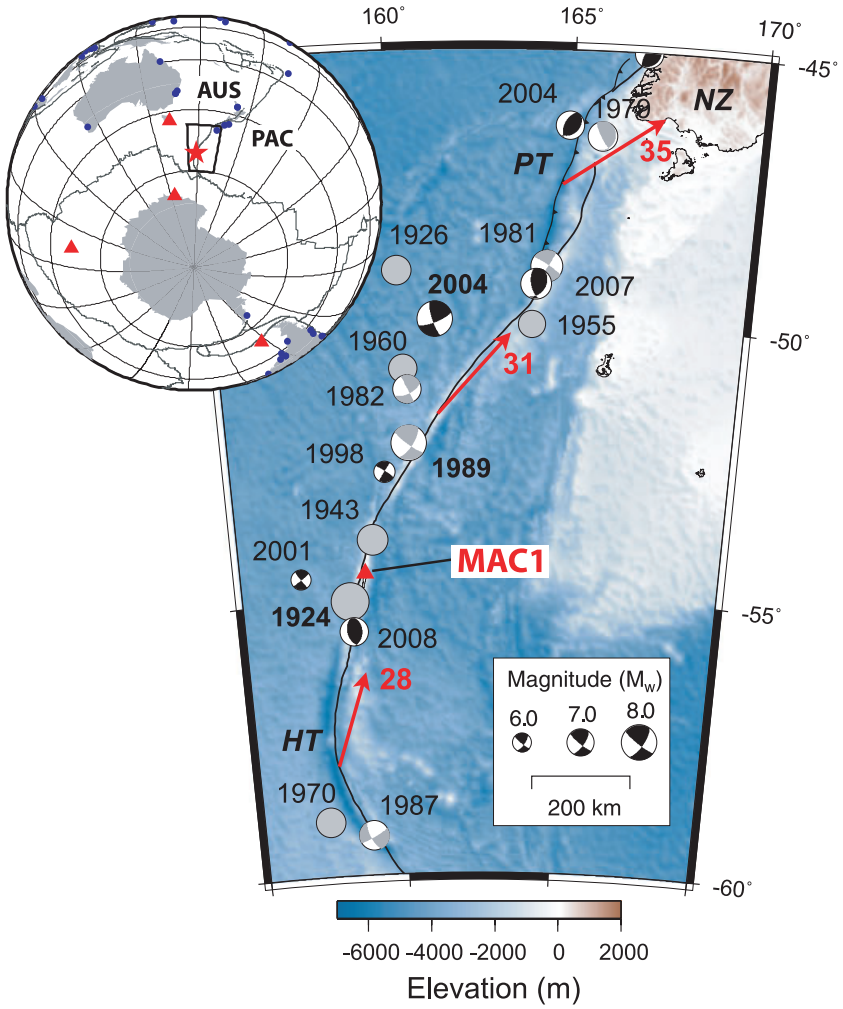

Figure 1. Macquarie Island locality map. Blue circles on the inset map represent tide gauges within the PSMSL with records greater than 40 yr. Red triangles represent sea level studies (completed and underway) that involve historical tide gauge observations. The main map shows the location of Macquarie Island (labelled MAC1) on the Macquarie Ridge Complex (MRC) south of New Zealand (NZ). Circles show locations and estimated moment magnitudes for $M_w > 7.0$ earthquakes that occurred during the 1912-present tide gauge record. Earthquake moment tensors and magnitudes are taken from the Global Centroid Moment Tensor catalogue for events since 1976. Black moment tensors denote earthquakes that occurred during the 1995-present GPS record, including two $M_w \sim 6$ events near Macquarie Island. Grey events pre-date the GPS record and solid circles come from the Pacheco & Sykes (1992) catalog. Red arrows and labels (mm/yr) show the predicted motion of the Australian Plate relative to the stable Pacific Plate at selected points from the ITRF05 poles of plate rotation. Labelled trenches are areas where lithospheric-scale convergence is inferred: HT, Hjort Trench; PT, Puysegur Trench.

the reduction of systematic error at the 100+ mm level during high sea states. Given frequent outages and sensor changes prior to 1998, we processed only data over the 10 years 1998–2007, estimating MSL from annual bins of data (some incorporating small data outages). The non-tidal residuals are highly negatively correlated with atmospheric pressure (correlation typically −0.7, standard deviations reduce from 0.12–0.14 m to 0.07–0.08 m following correction for the inverted barometer response). Given that we do not have a complete historical atmospheric pressure time-series that would allow the computation of inverse barometer corrections, we chose not to apply the inverted barometer correction to any of the tide gauge observations.

2.3 Datum connection

The tide gauge BM used during the AAE observational campaign consisted of an eye bolt and ring cemented into a rock in Garden Cove (Figs 2 and 3a). Photographs taken in 1975 (Fig. 3b) show that the eye bolt and ring corroded and broke away, leaving just the shaft of the bolt. The same photograph shows that the cement grout (clearly labelled BM AAE in Fig. 3a) had been reapplied in an assumed attempt to stabilize the BM. The change to the BM raises the question of the stability of the mark, including the possibility it was repaired but placed in a different position. To assess this question, photographs from 1912, 1975 and a third taken in 1992 (Fig. 3c) have been overlain for comparison, stretching the latter image to fit the original using a series of common features on the rock surface and a rubber sheeting transformation technique. Significant erosion is evident, including much of the rock surrounding the BM breaking away sometime prior to 1992 (Fig. 3), yet sufficient common features were present to tie the three images together to ascertain that the bolt lies within ±10 mm of the original position.

All sea level data collected prior to the modern era of observation have been connected to the AAE BM using traditional levelling techniques (Corcoran 1982; Doodson 1939; McCue 1971). Fortunately,

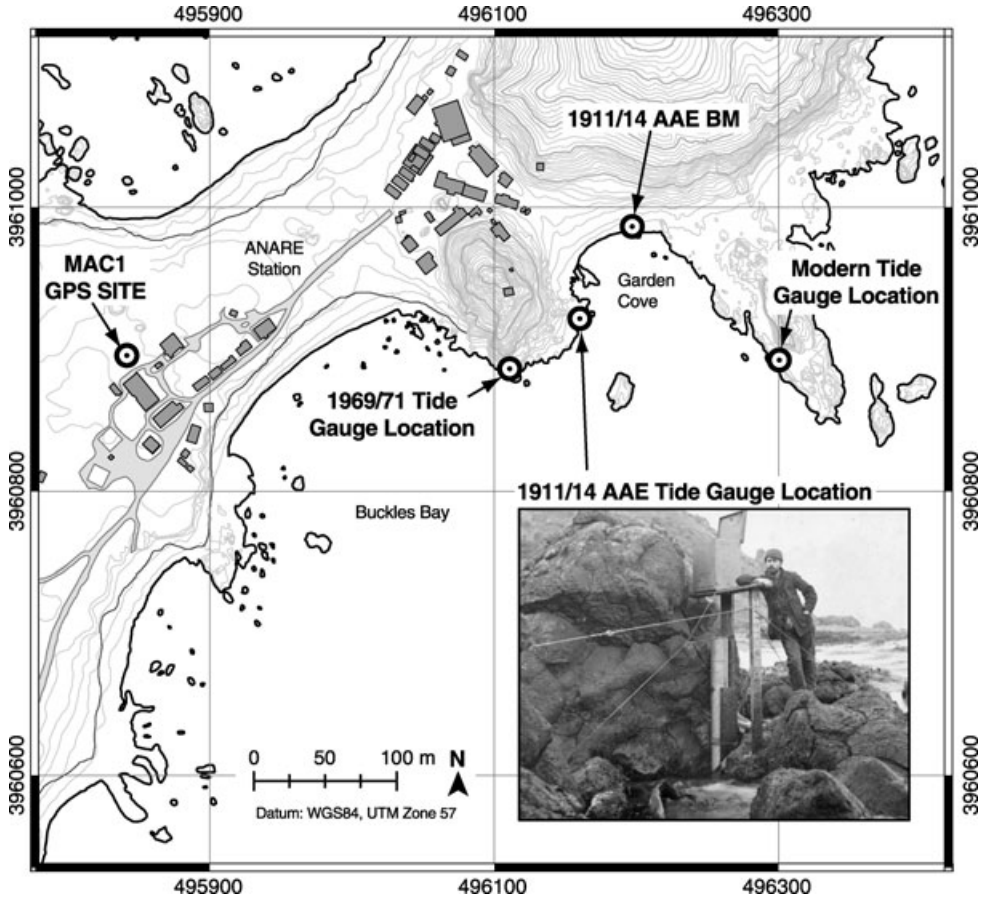

Figure 2. Location of the GPS station (MAC1), gauge locations (1911/1914, 1969/1971 and current), and the AAE benchmark location on the northern isthmus of Macquarie Island adjacent to the Australian National Antarctic Research Expedition (ANARE) station. Inset photograph shows Leslie Blake against the 1911/1914 tide gauge (photo Neg. Q843 C.A. Sandell, from Doodson, 1939).

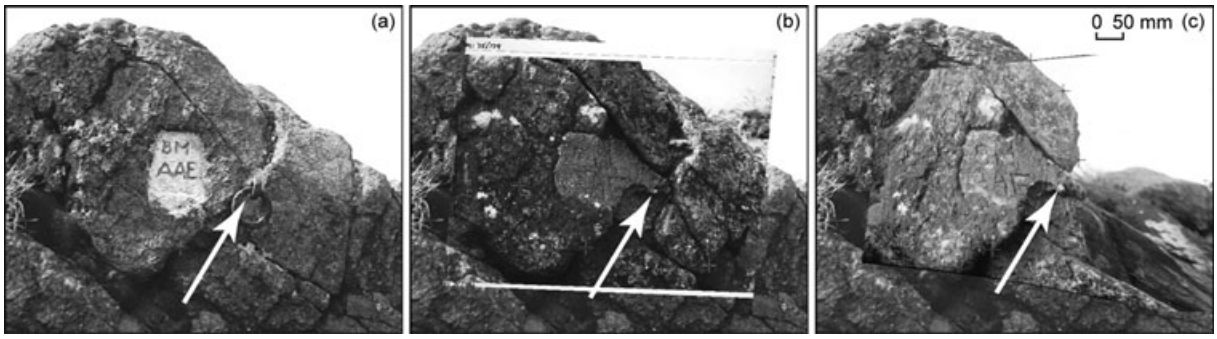

Figure 3. 1911/1914 AAE benchmark in Garden Cove. (a) Photograph taken 1912, (b) overlay taken in 1975 and (c) overlay taken in 1992. Note the new cement grout, erosion of the rock and loss of the eye bolt and ring. The arrow indicates the location of the shaft of the BM, scale is approximate.

modern benchmarks (BMs) were placed in adjacent rock and connected to the AAE BM in 1992 before the complete destruction of the AAE mark sometime prior to 2006. Level connections between these new marks, the modern tide gauges (the primary acoustic sensor and backup pressure sensor) and the MAC1 GPS site have been undertaken on several occasions. Results from seven independent levelling campaigns (Geoscience Australia 2008) confirm that there has been no significant differential motion between either of these tide gauge BMs or the BMs and the MAC1 GPS site some ∼450 m away.

2.4 Error estimates

Given the lack of observations over time and the brevity of the single 1912–13 MSL estimate, uncertainties placed on the annual (or near annual) MSL estimates must incorporate the expected contribution from inter-annual variability in sea level. Unlike other studies (e.g. Hunter *et al.* 2003), modern long-term sea level data (from a nearby long-term tide gauge, for example) are not available to assess the likely magnitude of this contribution. Instead, we analysed the time-series of satellite altimetry data from the TOPEX/Poseidon and

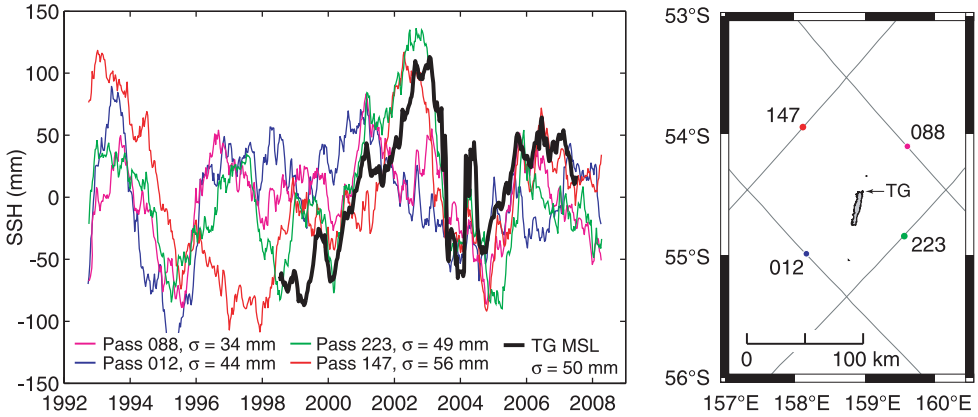

Figure 4. Left panel shows running annual mean sea surface heights (SSH) computed from multipass TOPEX/Poseidon and Jason-1 satellite altimetry (passes 147, 223, 088 and 012). The black line represents the running mean from the tide gauge data (mean offsets removed). Right panel shows the spatial location of ascending altimeter passes 147 and 223, descending passes 088 and 012, and respective points of closest approach with respect to the Macquarie Island tide gauge (TG).

Jason-1 missions (1992.7–2008.2), extracting data from the points of closest approach on the four passes adjacent to Macquarie Island. We used raw cycle-by-cycle data with standard corrections applied and ocean tides removed (our processing follows that of Leuliette *et al.* 2004). We compared running annual means computed using both the altimetry and tide gauge data (Fig. 4).

These results indicate that sea level at the tide gauge closely follows the open ocean, with the tide gauge record having the highest correlation to ascending altimeter passes 147 and 223. Given the agreement observed (Fig. 4), the standard deviation of the altimetry time-series can be interpreted as an uncertainty bound on each estimate of tide gauge derived MSL. The inter-annual variability in this region is very high in comparison with that reported in other studies (e.g. Testut *et al.* (2006) reported variability of 20–30 mm at Kerguelen Island). Our results are confirmed and further explained by Sokolov & Rintoul (2007), who described the complex frontal jets that comprise the Antarctic Circumpolar Current in this region of the Southern Ocean. The northwest to southeast orientation of these jets also offer possible explanation for the improved agreement between altimeter passes 147 and 223 and the tide gauge, versus passes 012 and 088 (Fig. 4). As a result of the analysis of the altimetry data, we adopted an uncertainty of ±50 mm (1-sigma) for each (annual) estimate of tide gauge derived MSL.

Given the discrete and irregular sampling of the MSL estimates in this study, the contribution of the nodal tide must be taken into consideration. The theoretical equilibrium amplitude of the 18.6 yr tide is 8.9 mm at this latitude (Pugh 1987). Despite being able to reliably determine the phase of the nodal tide, the amplitude remains highly uncertain (Pugh 1987). We chose to correct each estimate of annual MSL using the computed value of the nodal tide at the central time of the annual bin. To account for the large amplitude uncertainty, we computed the potential bias in the sea level trend using a nodal tide with a conservative uncertainty of ±8.9 mm (i.e. ±100% of the theoretical amplitude). Given the times of each MSL sample, the potential uncertainty in the sea level trend as a result of uncertainty in the nodal tide is ±0.064 mm yr^{-1} (this estimate is dealt with in the following section).

Uncertainty in the levelling connections between each various tide gauge and associated BMs is insignificant (i.e. likely to be <2 mm), with the exception of the ambiguity associated with point of reference used on the AAE BM. This combined with the marginally shorter observational span during the 1912–13 campaign, increases the uncertainty bound over this epoch to ±55 mm.

2.5 Relative sea level change

Analysis of the linear trend inferred from the annual estimates of MSL (corrected for the nodal tide), using a weighted least squares approach, yields an estimate of relative sea level rise of +4.8± 0.6 mm yr^{-1} (Fig. 5). For completeness, the uncertainty on this rate incorporates the in-quadrature addition of the uncertainty from the nodal tide (Section 2.4). The estimated rate is clearly higher than recent estimates of the global rate of absolute sea level rise of +1.7±0.5 mm yr^{-1} over the 20th century (Bindoff *et al.* 2007). Regional estimates computed from sea level reconstructions between 1950 and 2000 (Church *et al.* 2004) show rates close to +2.0 mm yr^{-1} in this region (higher than, but insignificantly different from the global average). The significant difference between estimates of relative and absolute sea level change is suggestive of possible land subsidence of the tide gauge. The magnitude of required subsidence is not explained by glacial isostatic adjustment (GIA), with global models predicting relative sea level rise at Macquarie Island of approximately 0.3 mm yr^{-1} (e.g. Davis & Mitrovica 1996; Milne *et al.* 2001; Church *et al.* 2004; Peltier 2004). Given the small magnitudes of these predictions and their uncertainty in a poorly constrained part of the Earth, we assume for the purposes of this study that the effect is insignificantly different from zero. In the following section, we investigate the recent tectonic evolution of the site.

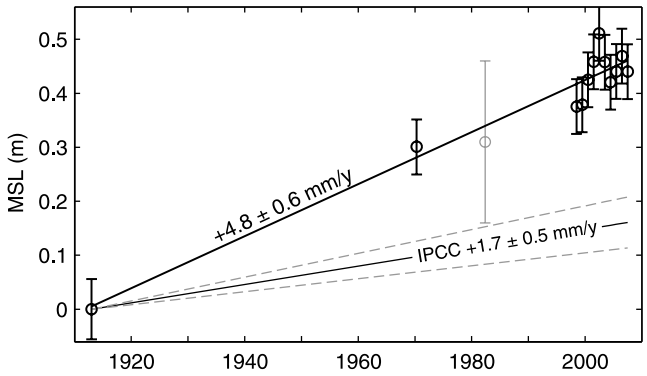

Figure 5. Relative sea level trend at Macquarie Island and the comparative absolute global MSL trend over the 20th century (Bindoff *et al.* 2007).

3 LAND MOTION ESTIMATES

3.1 Tectonic setting

Macquarie Island is the culmination of a bathymetric ridge known as the MRC that is situated along the Australia–Pacific Plate boundary. In the past 20 Myr, the MRC portion of the plate boundary has transitioned from mid-ocean ridge spreading through strike-slip to the current state of dextral transpression, with incipient subduction established along portions of the boundary (Massell *et al.* 2000; Lebrun *et al.* 2003; Cande & Stock 2004; Meckel *et al.* 2005; Hayes *et al.* 2009). Analyses of raised beach terraces suggest that the Island has emerged at a rate of uplift of 0.8 mm yr^{-1}, averaged over the past 340 Kyr (Adamson *et al.* 1996). The MRC region has been the location of numerous historical earthquakes, including two of the largest transform earthquakes in the instrumental record; the M_w ~8.1 earthquakes of 1989 and 2004. Focal mechanisms show that the majority of large earthquakes in the region are consistent with dextral strike-slip along the plate boundary fault with a smaller number of thrust-style events (Fig. 1; Ruff *et al.* 1989; Frohlich *et al.* 1997; Moore *et al.* 2000; Hayes *et al.* 2009). A significant fraction of the region's seismic moment release has occurred west of the main plate boundary, likely on relict fracture zones (Valenzuela & Wysession, 1993). These earthquakes have been interpreted as accommodating strain between the stable Australian Plate and an independent Macquarie Plate and/or within a deforming Puysegur Block (Cande & Stock 2004; Hayes *et al.* 2009). Estimates of vertical deformation from regional earthquakes at the tide gauge are crucial for understanding the absolute sea level change component of the observed relative sea level record.

3.2 Space geodetic estimates of land motion

The longer term geological evidence suggests that Macquarie Island has uplifted at an average rate of 0.8 mm yr^{-1} over the past 340 Kyr (Adamson *et al.* 1996), yet our relative sea level data ($+4.8 \pm 0.6$ mm yr^{-1}) suggest that the Island has, on average, subsided over the last century when compared with the global rate of sea level rise (Fig. 5). Analysis of GPS data, including that from the MAC1 GPS site in operation since 1995, provides a contemporary estimate of crustal motion at this location. We begin this part of the investigation with an analysis of the MAC1 time-series in the vertical component (Fig. 6), as provided by four different GPS analyses expressed with respect to the 2005 release of the International Terrestrial Reference Frame (ITRF2005, Altamimi *et al.* 2007). For comparative purposes, we include time-series from the

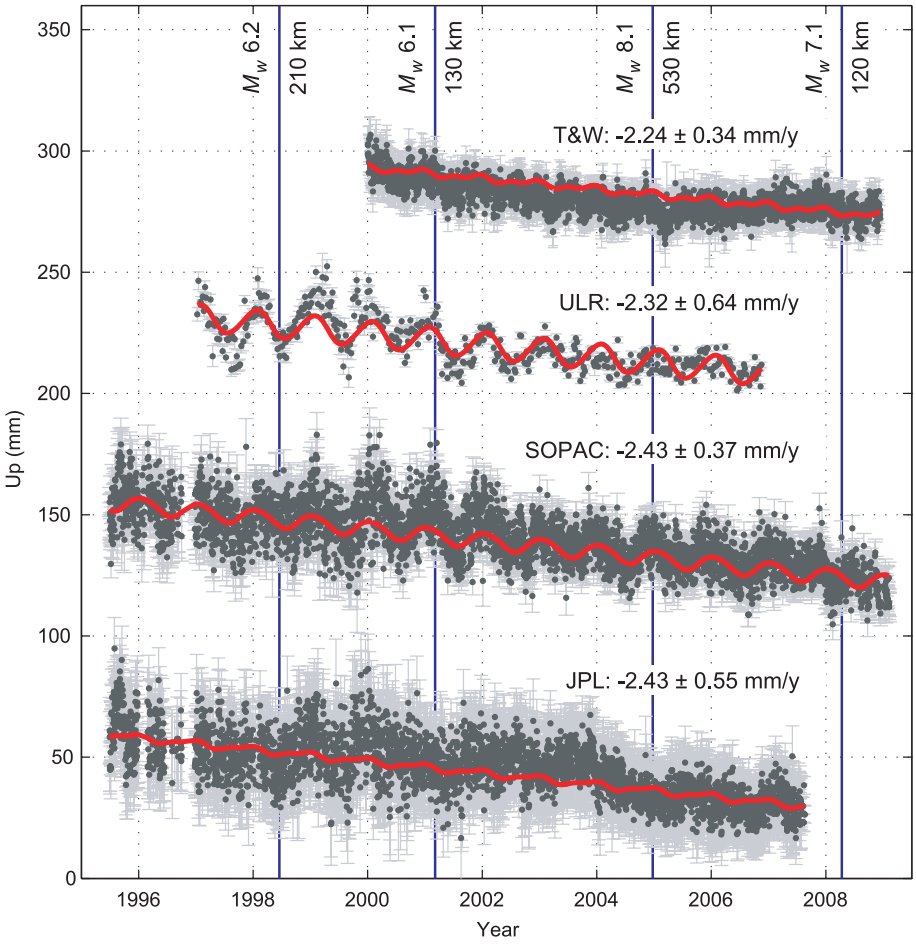

Figure 6. MAC1 vertical time-series relative to the nominal ITRF2005 from four separate GPS analyses (see text for details). Arbitrary offsets have been applied for clarity. The red line on each solution represents a linear model that incorporates periodic components at solar annual and semiannual periods and estimated using the full time-series for each solution. The uncertainties about the stated trends were computed using a combined time-variable white and power-law noise model using the CATS software (Williams, 2008). The time of earthquakes coincident over the period are indicated with vertical blue lines, with moment magnitudes and distances to the epicentres indicated at the top of the figure.

solutions of the Jet Propulsion Laboratory (JPL; http://sideshow.jpl.nasa.gov/mbh/series.html), Scripps Orbit and Permanent Array Center (SOPAC; http://garner.ucsd.edu/pub/timeseries/), Université de La Rochelle consortium (ULR; Wöppelmann *et al.* 2009) and The Australian National University/University of Tasmania (T&W; Tregoning & Watson 2009). The solutions of T&W, SOPAC and JPL are daily estimates (one coordinate estimate per 24 h), whereas ULR have combined their daily solutions to generate a time-series of weekly coordinate estimates.

On first inspection the four time-series (Fig. 6) show a broad level of agreement with respect to the estimated linear rate of subsidence. All solutions yield statistically insignificant estimates of coseismic displacement in the vertical component for the earthquake events shown in Fig. 6. Both the JPL and SOPAC solutions show considerably higher noise and significant non-linear behaviour (e.g. at ∼2004.0 in the JPL time-series). Considerable energy at an annual period is evident in both the SOPAC and ULR solutions (also within the JPL solution but obscured by step changes most likely to be caused by a non-homogeneous processing methodology over the duration of the time-series). This energy is likely to reflect deficiencies in the modelling of the delay induced by the troposphere, specifically relating to the methods adopted in the T&W solution to compute the zenith hydrostatic delay and the mapping function used to relate the observed slant path delay to the zenith direction (Tregoning & Watson, 2009). Although considerably less energetic at annual periods, the T&W solution remains non-linear over the full duration of the series, with an interesting point of inflection around ∼2005 following the 2004.9771 earthquake. This is of considerable relevance to this study as discussed in the following sections. Tregoning & Watson (2009) provide a rigorous quantitative assessment of cumulative enhancements included within the solutions, specifically addressing *a priori* zenith hydrostatic delays, loading of the crust due to the Earth's atmosphere, and refinements to the mapping functions. We use in this study the homogeneously reprocessed GPS time-series of Tregoning & Watson (2009), updated to incorporate sites throughout New Zealand and southeastern Australia, and processed using the GAMIT/GLOBK analysis suite (Herring *et al.* 2008).

During the period of the GPS record at MAC1 there have been four large earthquakes in the vicinity of Macquarie Island: M_w 6.2 (1998.4559), M_w 6.4 (2001.1764), M_w 8.1 (2004.9771) and M_w 7.1 (2008.2787). Of these events, only the distant great earthquake of 2004 caused significant coseismic deformation in the horizontal components of the T&W time-series. The M_w 6.2 event of 1998.4559 (predating the T&W time-series) also failed to generate any observable coseismic displacement across any coordinate components of the other GPS solutions presented in Fig. 6. This observation gives us confidence that the available twentieth century earthquake catalogue, nominally complete for $M_s > 7.0$ (Pacheco & Sykes 1992), most probably contains all of the events likely to have been sources of vertical land motion at the tide gauge site since the initial installation of the AAE tide gauge in 1912.

3.3 2004 Earthquake coseismic displacements

The largest earthquake that has occurred in the Macquarie Island region since the installation of the continuous GPS receiver is the M_w 8.1 event of 2004 December 23, preceding the great Sumatra earthquake by 2.4 days. In contrast to the similar magnitude 1989 earthquake, which was located on the MRC, the centroid of the 2004 event occurred over 130 km west of the plate boundary, ∼530 km north of Macquarie Island (Fig. 1; Hayes *et al.* 2009). This dominantly strike-slip earthquake produced a tsunami that arrived in southern New Zealand and Tasmania with peak to trough ranges of approximately 30 and 20 cm, respectively (National Tidal Centre 2005).

We estimated the coseismic displacement at 16 regional continuous GPS sites (Fig. 7). We calculated median positions with associated uncertainties for north, east and up components from de-trended daily time-series for 7-day intervals immediately preceding and following the day of the earthquake. The 7-day window length represents a compromise in minimizing biases caused by daily variability, longer period time-correlated noise and post-seismic deformation. None of the sites in the regional network have vertical offsets that are statistically distinct from zero but significant horizontal displacements occurred, characteristic of far-field elastic earthquake deformation (Figs 7 and 8).

We inverted the GPS coseismic displacements to estimate rupture parameters for the 2004 MRC event using an elastic half-space dislocation model (Okada 1992). In light of the limited and distant geodetic observations and uncertainty in the source fault geometry, we modelled the earthquake as a single, rectangular rupture plane with uniform slip, estimating the location and orientation of the plane and the orientation and magnitude of slip. We used bounded non-linear least squares to estimate the source parameters, constraining the general location of the rupture plane using the hypocentre location and associated uncertainty from the U.S. Geological Survey National Earthquake Information Center (USGS). We performed the model optimization using 100 realizations with different random sets of initial parameter values to ensure that we found the minimum misfit in the parameter space. The inversion of the far-field displacements is only slightly sensitive to the dip, depth and length of the rupture, and the bounds we place on these parameters provide estimates that are compatible with the geologic setting of the earthquake. We limit the basal depth of the rupture to 27 km or less, following a global relationship for earthquake depth and age of oceanic lithosphere (McKenzie *et al.* 2005).

Predictions from the best fitting model fit the observed horizontal displacements at the 1-sigma level for nearly all of the sites, with a mean residual of 1.6 mm (Fig. 7). The model marginally over estimated the coseismic deformation in the vertical component at MAC1, with a predicted deformation of −8 mm (the observed deformation was insignificantly different from zero with an uncertainty at the 4 mm level). Despite the observed negligible instantaneous vertical offset (in contrast to that seen in both the horizontal components), the T&W GPS record at MAC1 shows negative values in the months following the earthquake reaching a minimum of ∼−7 mm at 2005.2, compared to the pre-earthquake mean value (Fig. 6). However, we regard such estimates of coseismic static vertical deformation as equivocal, given the delay of this signal and the nature of time-correlated noise elsewhere in the time-series.

The centroid of our best fitting model rupture (49.838°S, 161.378°E) is located around 12 km from the Global Centroid Moment Tensor Project (CMT) solution, and similarly close to the centroid of Hayes *et al.* (2009). The symmetry of predicted far-field elastic deformation at the GPS sites precludes favouring one nodal plane over the other on the basis of the GPS data. Likewise, the lack of directivity in the seismological observations does not resolve a unique fault plane orientation, although the generally north–south alignment of aftershocks favours the left-lateral plane (Hayes *et al.* 2009). Our estimated location lies near a major fracture zone in the Australian Plate (the 'Lhuwa' fracture zone of Massell *et al.* 2000).

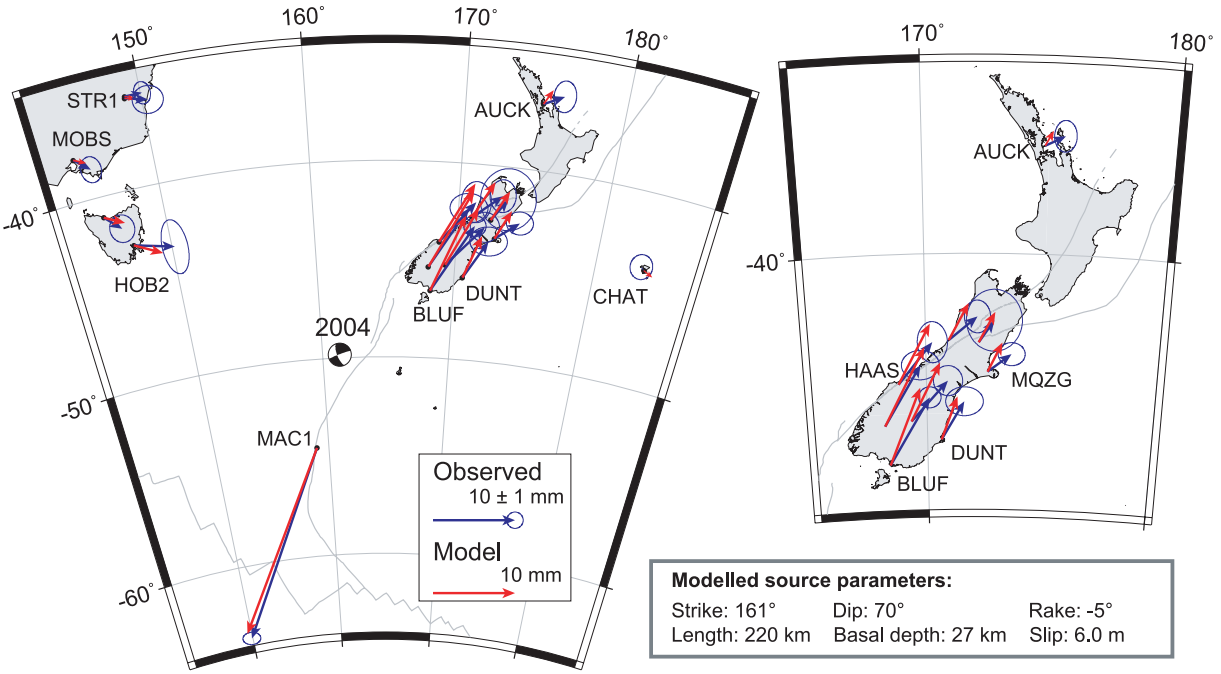

Figure 7. Observed and modelled horizontal coseismic deformation from the great M_w 8.1 earthquake of 2004 December 23. The observed coseismic deformation at MAC1 was approximately 24.6 mm with an orientation of 204°. The right panel shows an enlarged view of deformation across New Zealand (note the vector scale remains constant across both panels).

The fracture zone is curved, but the modelled strike of 161° approximates the overall trend of the fault trace in this area. Slip on this southeast-striking nodal plane is left-lateral, at a high angle to the right-lateral slip vector on the ∼35° striking main plate boundary in the 1989 event (Fig. 1). The GPS data are best fit by a moment closer the USGS moment tensor value (M_w 8.0) than the CMT estimate of M_w 8.1.

3.4 2004 Earthquake post-seismic deformation

In the years following the 2004 earthquake, the horizontal components of the MAC1 GPS time-series show continued deformation over time in the same direction as the coseismic displacement (Fig. 8—note each coordinate component has been detrended using the rate determined prior to the 2004 earthquake). This post-seismic deformation from 2004.9771 to 2009 is approximately equal in magnitude to the coseismic offsets. The lower signal-to-noise ratio for the vertical component makes the vertical post-seismic behaviour more difficult to interpret. The GPS solution shows a change in the rate of vertical motion near the time of the Macquarie 2004 earthquake, with the inflection suggesting post-seismic uplift relative to the pre-earthquake rate of subsidence. This is clearly evident in Fig. 6, highlighted by the poorly fitting linear plus periodic model (red line in the T&W time-series of Fig. 6).

Before further investigating this rate change, it is important to quantify the absolute vertical velocity prior to the 2004 earthquake, a period in which the GPS vertical time-series is well represented by a linear model. To maintain consistency between the T&W and the other three time-series, we presented the data in Fig. 6 with respect to the published ITRF2005 (Altamimi *et al.* 2007); however, Tregoning & Watson (2009) made a modification in their implementation of ITRF2005 to account for a Z-translation rate difference between ITRF2005 and the older ITRF2000 (Altamimi *et al.* 2002). Much of the recent literature continues to present rates consistent with ITRF2005 (e.g. Wöppelmann *et al.* 2009), despite some studies showing that the long-term centre of mass of the earth is more consistent with the definition of ITRF2000 (Argus 2007; Argus *et al.* 2010). For the estimation of an absolute trend in the vertical component, we favour applying a correction consistent with Argus (2007), implying that ITRF2005 velocities are over-estimated by an amount equating to approximately 1.8*sin(lat) or ∼1.46 mm yr^{-1} at Macquarie Island. As per Tregoning and Watson (2009), we make this correction to each site used in the GPS analysis just prior to realizing the reference frame within GLOBK (Herring *et al.* 2008).

Given the time correlated noise structure inherent in GPS time-series, we derive our vertical rate from the resultant time-series for the period up until the 2004 earthquake using a combined time-varying white and power-law noise model within the CATS software (Williams 2008). The time-varying component to this noise model is important given the gradual improvement in ambiguity resolution over time (Tregoning & Watson 2009). This results in a reduction in formal coordinate uncertainty estimates over time, which must be taken into consideration in any regression analysis. The resultant vertical subsidence at MAC1 prior to the 2004 earthquake was determined to be -2.46 ± 0.64 mm yr^{-1}.

Post-seismic deformation caused by continued after-slip on the rupture surface or its deeper extension produces post-seismic subsidence at MAC1; however, viscoelastic relaxation of the upper mantle can produce uplift or subsidence, depending on the upper mantle rheology. Because none of the available GPS solutions show enhanced rates of post-seismic subsidence, we conclude that the deformation at MAC1 is more likely due to viscoelastic relaxation of the upper mantle.

Post-seismic uplift in a quadrant that experienced far-field coseismic subsidence is diagnostic of a less viscous layer sandwiched between stronger materials (Hearn 2003). In an oceanic setting, the asthenosphere is a weaker layer between the lithosphere above and

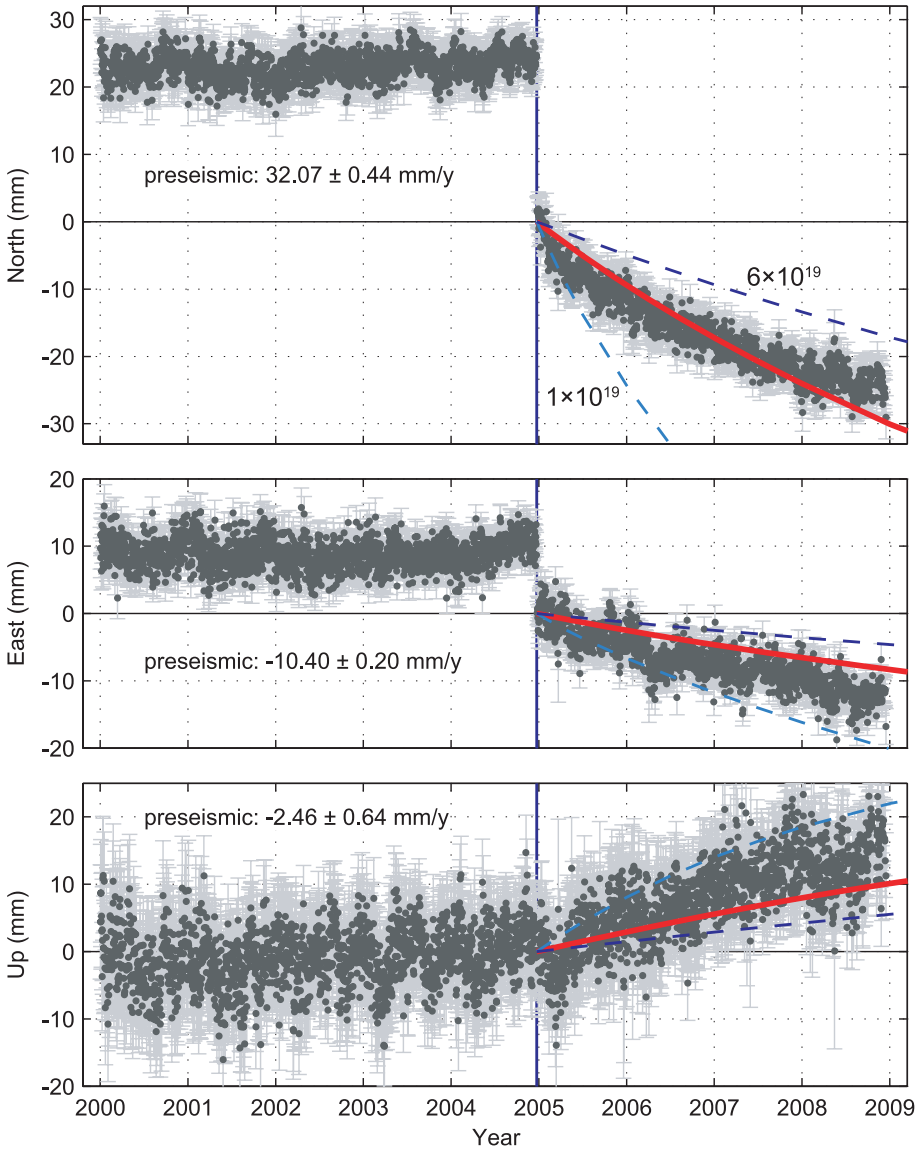

Figure 8. Observed coseismic and post-seismic deformation (north, east and up from the T&W GPS solution) at the MAC1 site from the great M_w 8.0 earthquake of 2004 December 23. The time-series have been de-trended using the preseismic velocity (as indicated in each panel). The vertical blue line indicates the time of earthquake, the red line represents the best fitting post-seismic model (asthenospheric viscosity of 3 $\times$ 10^{19} Pa s) and the dashed blue lines represent bounds on the asthenospheric viscosity used in the modelling (labelled in top panel; see text for details).

stronger upper mantle below. Viscoelastic deformation in a system with this type of stratification was used by Pollitz *et al.* (1998) to explain post-seismic seismicity rates in the Pacific Ocean basin.

To determine the rheological structure responsible for the observed post-seismic deformation at Macquarie Island, we used VISCO1D, a layered, spherical, post-seismic viscoelastic deformation model, which accounts for gravitational effects (Pollitz 1997). We used the earthquake geometry and slip obtained from the coseismic modelling to characterize the rheological structure responsible for the observed post-seismic deformation at Macquarie Island. We used a rheological layering based on that used by Pollitz *et al.* (1998), with a 60-km-thick elastic lithosphere overlying a viscoelastic asthenosphere. Evidence for the presence of a sharp lithosphere–asthenosphere boundary has been strengthened by a receiver function study of oceanic borehole seismometer data (Kawakatsu *et al.* 2009). They found an age-dependence for the thickness of oceanic lithosphere that roughly follows predicted isotherms from thermal modelling, and they suggested that the sharp upper boundary of the asthenosphere is controlled by the limit of partial melting in the upper mantle. The age of the crust at the centroid of the 2004 earthquake is approximately 31 Ma (Keller 2004). Based on the data of Kawakatsu *et al.* (2009), the thickness of the lithosphere of this age is approximately 60 km. The youngest measured ages of rocks on Macquarie Island are 6–10 Ma (Duncan & Varne 1988; Wertz 2003), and the lithosphere is likely thinner there. However, the tectonic reconstructions of Meckel *et al.* (2005) predict a cumulative convergence at the latitude of Macquarie Island of 90 $\pm$ 60 km, which would cause thickening of the lithosphere. With the lack of more detailed lithospheric thickness information in this region, we assume that laterally homogenous layering is appropriate. Another oceanic borehole seismometer study inferred the base of the upper mantle seismic low-velocity zone occurs at a depth of ~200–210 km (Shinohara *et al.* 2008). We used a depth of 200 km for the base of the asthenosphere, where the viscosity

increases by a factor of 100 compared to the value of the asthenosphere above. This thickness of the asthenosphere and viscosity contrast at its base is also broadly consistent with plate tectonic and GIA modelling (Paulson & Richards 2009). We used a linear Maxwell rheology for the upper mantle, because fewer rheological parameters are required to characterize the system.

Post-seismic deformation is evident in the time-series of several of the nearest regional GPS sites (including the long running IGS HOB2 site located adjacent to the HOBART26 VLBI site in southern Tasmania on the Australian continent). In contrast to MAC1, all of these sites are located on continental crust, and their post-seismic behaviour is likely influenced by lateral variations in rheology relative to that at Macquarie Island. In addition, the signal-to-noise ratio is much lower for the observed post-seismic deformation at HOB2 and the two southern New Zealand sites (DUNT and MQZG) with sufficient data for determining accurate preseismic station velocities. For these reasons, we used only the data at MAC1 for the model optimization. We modelled the post-seismic deformation at MAC1 with the mantle viscosity as a free parameter that we allowed to vary over three orders of magnitude. We found the best fit to the post-seismic time-series with an asthenospheric viscosity of 3×10^{19} Pa s. The model fit to the observed post-seismic time-series at MAC1 explains the majority of the variance, particularly for the north and vertical components (red line, Fig. 8). Bracketing scenarios from higher and lower viscosities (dashed blue lines, Fig. 8) show the post-seismic data are sensitive to differences in viscosity at the 1×10^{19} Pa s level around the best estimate. The inferred viscosity appears robust to some of the more poorly resolved details of the coseismic fault plane. For example, varying the basal depth of the coseismic rupture in the depth range of the upper half of the lithosphere does not change the inferred asthenospheric viscosity at the one significant digit level.

The predicted ratio of east to north deformation is lower for our viscoelastic model than for an afterslip model, suggesting that invoking an additional process might yield a better fit to the data. Likewise, the modelled north component of the deformation has less curvature than the observed data. This may reflect an initial period of post-seismic after-slip or that the upper mantle would be better described by a bi-viscous Burger's-body rheology (e.g. Bürgmann & Dresen 2008). However, we feel that the fractional gains in model fit offered by invoking more complex processes do not support the addition of unknown parameters, given that we only have the time-series of one site to invert.

The significant differences in rates of deformation at MAC1 before and after the 2004 earthquake (particularly for the vertical component), suggest that the similar magnitude, and closer, 1989 and 1924 events (Fig. 1) likely dominate the twentieth century evolution of vertical deformation at Macquarie Island. In the following sections, we use available seismological constraints together with the deformation models used for the 2004 earthquake to constrain the potential amount of vertical deformation at Macquarie Island from the earlier earthquake events.

3.5 1989 Earthquake deformation

Numerous seismological studies analysed the source parameters of the 1989 May 23 Macquarie Ridge earthquake (Braunmiller & Nabelek 1990; Ekström & Romanowicz 1990; Satake & Kanamori 1990; Tichelaar & Ruff 1990; Anderson & Zhang 1991; Das 1992, 1993; Velasco *et al.* 1995). Most of these studies concluded the fault plane had a strike similar to the plate boundary at the epicentre (030°–040°), steeply dipping either west or east, and a nearly pure right-lateral slip vector. The range of reported seismic moments varies from 1.3×10^{21} N m to 2.4×10^{21} N m (M_w 8.0–8.2), with the higher estimates corresponding to greater inferred downdip widths of the rupture plane. Reported rupture depths range from 10 to 50 km. This great earthquake produced relatively few aftershocks for its size, many of which occurred off of the main plate boundary fault, including several inferred to be left-lateral slip on a fracture zone in the Australian Plate (Das, 1992). The orientation and sense of slip of the left-lateral 1989 aftershocks is similar to what we infer for the 2004 mainshock. Based on the distribution of the most concentrated aftershocks on the plate boundary, many authors estimated a total rupture length of only 100–120 km. Das (1993) favoured a 230 km rupture length, with a termination ∼120 km to the southwest of the other studies, near a few aftershocks and a segment boundary defined by an extensional step-over and a ∼18° change in strike of the plate boundary.

We used these published seismic observations to constrain a likely range of earthquake parameters for the 1989 event. Based on the trend of the plate boundary fault in the vicinity of the epicentre we used a strike of 032°. We used a vertical dip, given uncertainties in the dip direction and the overall pattern of steep inferred nodal planes. One of the most important controls on the deformation at Macquarie Island is the proximity of the southern end of the earthquake rupture. To address the uncertainty in this parameter, we considered two bracketing scenarios: a 120-km length corresponding to the densest aftershocks, and a 220-km rupture that terminates at the step-over in the Macquarie Ridge, following Das (1993). We accounted for the wide range of reported depths by using basal rupture depths of 20 and 40 km. Average slip magnitudes were calculated from the fault areas and a generalized range of seismic moments. For the shallower case, we used 1.3 and 1.8×10^{21} N m and 1.8 and 2.4×10^{21} N m for the deeper fault. Elastic half-space dislocation modelling of these earthquake scenarios predict coseismic vertical deformation at Macquarie Island of −4 to −17 mm, with greater subsidence corresponding to the longer rupture, larger moment and shallower fault.

We used the same range of rupture scenarios to estimate a likely range of post-seismic vertical deformation at the Macquarie Island tide gauge, employing the viscoelastic rheological layering determined from the inversion of post-seismic deformation caused by the 2004 earthquake. Macquarie Island lies in the compressional quadrant of both the 2004 and 1989 strike-slip earthquakes, and the predicted sense of far-field elastic coseismic deformation is subsidence for both cases. However, for the longer rupture scenarios for the 1989 earthquake, Macquarie Island lies in a zone of post-seismic subsidence, whereas the viscoelastic modelling predicts post-seismic uplift for the 2004 event (Fig. 9).

Using these different scenarios, the integrated total deformation at Macquarie Island from the 1989 earthquake through to 2009.0 ranges from −95 to 18 mm. The mean rate of 1989 post-seismic deformation in the period 2000–2004.9771, the interval over which we estimated the pre-seismic velocity of MAC1 (-2.46 ± 0.64) ranges between 0.0 to −4.7 mm yr^{-1}. Similar to the coseismic modelling, the greatest post-seismic subsidence estimates at MAC1 are produced by the longer rupture, greater moment and shallower rupture depth.

3.6 1924 Earthquake deformation

The epicentre of the 1924 June 26 earthquake is the closest to Macquarie Island of all of the large seismic events that occurred over

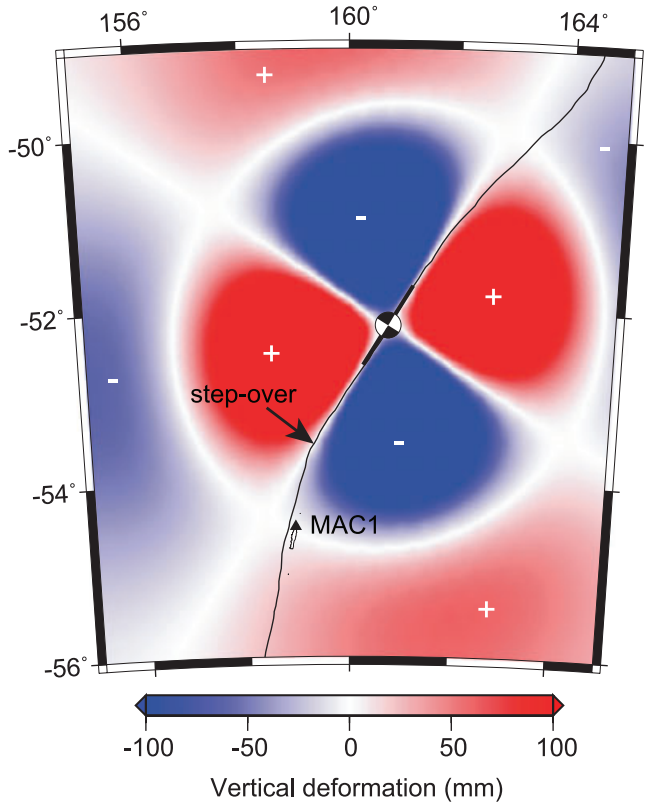

Figure 9. Predicted viscoelastic post-seismic deformation in the vertical component, accumulated from the 1989 event through to 2009.0. The fine black line shows the main plate boundary fault, and the heavy line is the trace of the modelled 120-km-long rupture. Longer rupture scenarios that extend southwest to the step-over broaden the region of near-field subsidence to include Macquarie Island.

the duration of the tide gauge record (Fig. 1), but there are fewer data to constrain the location and source parameters of this event compared to the more recent MRC seismicity. Ruff *et al.* (1989) relocated the epicentre of this earthquake to 55.0 ± 0.5°S, 158.4 ± 1.7°E (Fig. 1), north of the 56.0°S latitude of Gutenberg & Richter (1949). The Ruff *et al.* (1989) epicentre location lies north of the Hjort trench and the northern uncertainty limits include the southern portion of Macquarie Island. Ruff *et al.* (1989) presented a partial focal mechanism for the 1924 event with one of the nodal planes dipping steeply westward and striking approximately north. The polarities of the available first motion observations are incompatible with right-lateral slip on a high-angle structure subparallel with the plate boundary. Assuming a pure thrust slip vector, the focal sphere observations are compatible with a thrust striking 010° (parallel to the local orientation of the plate boundary), and dipping to the east between 15° and 20°. Meckel *et al.* (2003) interpreted that the oblique convergence at the Hjort trench was accommodated by deformation partitioned between a high-angle strike-slip fault and a low-angle decollement, where the Australian Plate is being underthrust beneath the Pacific Plate, based on bathymetric and seismic observations. The thrust fault is less distinct to the north of the bathymetric Hjort trench, but they suggested that it extends as far as ∼55°S. Based on the focal mechanism, we interpret that the 1924 earthquake occurred on this shallowly east-dipping major thrust fault.

In addition to the uncertainties regarding the location and sense of the 1924 earthquake rupture, the available seismic estimates of its magnitude span a wide range. In the Pacheco & Sykes (1992) earthquake catalogue, the 1924 Macquarie event is reported as M_s 7.5, reinterpreted from the M_s 7.7 value of Abe (1981). Pacheco & Sykes (1992) also estimated a seismic moment of 3.02×10^{21} N m (M_w 8.3) for this event, based on a calibration of mantle Rayleigh wave amplitudes reported by Brune & King (1967). The Ekström & Dziewonski (1988) relationship between M_s and seismic moment that Pacheco & Sykes (1992) found valid for most earthquakes $M_s < 8.0$ yields an estimated moment of 2.5×10^{20} N m. This full order of magnitude uncertainty in seismic moment translates to similar scale uncertainty in the surface deformation effects of the earthquake at Macquarie Island.

Elastic modelling of hypothetical large moment thrust ruptures on the ∼300-km-long Macquarie segment, centred on the Ruff *et al.* (1989) epicentre, predicts coseismic uplift of >1 m at Macquarie Island. This scenario seems incompatible with the ∼20 cm of subsidence over the period 1912–1970 implied by the rate of the relative sea level record (Fig. 5). Consequently, we focused on rupture scenarios with the Ruff *et al.* (1989) epicentre near the northern edge of the rupture plane. A large thrust earthquake on the plate boundary south of Macquarie Island primarily would have occurred on the Hjort trench segment where a lithospheric–scale thrust has been inferred (Meckel *et al.* 2003). In this scenario, Macquarie Island lies in an area of both coseismic and post-seismic subsidence. As with the 1989 earthquake, the amount of deformation caused by the 1924 earthquake scales strongly with both the moment and the proximity of the end of the rupture to the tide gauge (Fig. 10). Plausible earthquake scenarios predict up to 50 cm of subsidence by 2010 from combined coseismic and post-seismic deformation from the 1924 earthquake. Using the viscoelastic layering inferred from the 2004 earthquake, post-seismic modelling suggests that the rates of post-seismic subsidence from the 1924 earthquake remain significant at present, and may dominate the total twentieth century vertical deformation budget (Fig. 10).

4 ABSOLUTE SEA LEVEL CHANGE AND CONSTRAINTS ON EARTHQUAKES

Our modelling of the three $M_w \geq 7.5$ earthquakes that occurred in the region of the Macquarie Island tide gauge during its operation suggests that potential tectonic deformation is sufficient to explain the departure of the relative sea level change from sensible limits that take into account regional variability either side of the globally averaged absolute rate of sea level rise. The combined constraints from the long relative sea level record and the recent GPS estimates of crustal velocity place limits on the likely rate of absolute sea level rise at Macquarie Island, as well as the magnitudes and extents of the great earthquake ruptures over the twentieth century.

The timescales over which the post-seismic vertical deformation rates change are long relative to the tide gauge record (Fig. 10). As post-seismic deformation from the 1924 earthquake appears to be the most likely cause of land subsidence between the first and second tide gauge deployments, the 1924 earthquake is also likely to be the dominant cause of continued subsidence since 1970. Based on predicted total vertical deformation, many potential scenarios for the 1924 and 1989 great earthquakes can be excluded due to poor agreement with the relative sea level time-series or the modern GPS record.

Fig. 11(a) shows three examples of assimilated earthquake time-series that are compatible within reasonable limits of the observed GPS vertical velocity in the period 2000–2004.9771. These

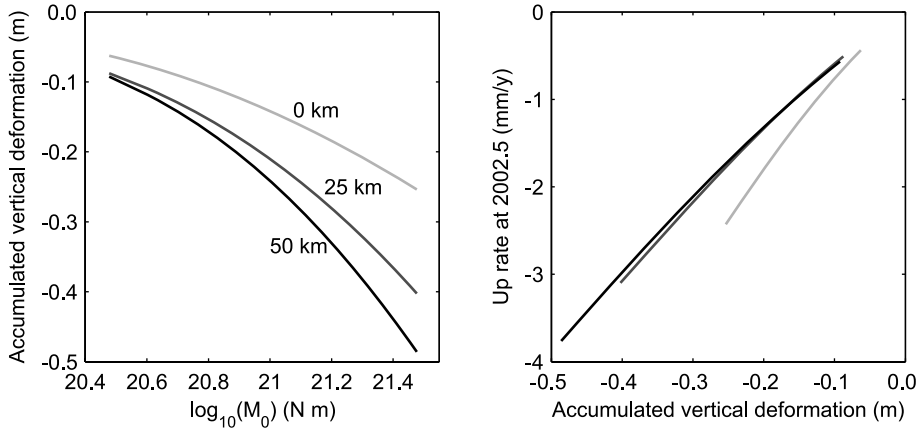

Figure 10. Predicted deformation at Macquarie Island tide gauge from the 1924 earthquake. The left panel shows total vertical deformation (including coseismic) from the time of the earthquake through 2010 as a function of seismic moment. The three curves show predictions for three distances from the Ruff *et al.* epicentre to the northeastern edge of the rupture (greater distance northeast from the epicentre is closer to Macquarie Island). The right panel shows the predicted strong correlation between the total deformation and the rate of subsidence (shown here at 2002.5) caused by ongoing viscoelastic relaxation from the earthquake.

time-series assume that the orientation of the thrust fault plane we infer from the Ruff *et al.* (1989) first motion observations is approximately correct for the 1924 earthquake. Modelled 1924 earthquake scenarios 1 and 2 (M_w 8.2 and 8.1, respectively) predict vertical deformation from this event alone in the period 2000–2004.98 (the period from which we estimate the pre-2004.9771 earthquake velocities from the GPS record) of -2.5 and -1.9 mm yr^{-1}. These rates are nearly the total observed vertical velocity of MAC1 prior to the 2004 earthquake (-2.46 ± 0.64 mm yr^{-1}), which suggests that the contribution of the more distant 1989 earthquake was relatively minor. Less deformation from the 1989 earthquake implies that the shorter rupture inferred from the most dense region of aftershocks is most likely, or at least that the majority of the slip was concentrated in the vicinity of the epicentre (Fig. 9). These observations favour the lower range of estimated moments for the 1989 earthquake as well. Adding in the modelled post-seismic deformation for the low moment, short rupture 1989 earthquake yields total pre-2004.98 earthquake vertical rates of -3.1 and -2.5 mm yr^{-1} for these scenarios (Fig. 11a). We regard scenario 1 as an upper limit to the amount of earthquake-generated subsidence at the tide gauge that is permissible within the uncertainties in the GPS record. This therefore implies a lower bound on the absolute rate of sea level rise at this location. Scenario 3 (1924 earthquake M_w 8.0) represents an attempt to reproduce the lower limit of the rate of GPS-observed subsidence between 2000 and 2004.98. The rate for scenario 3 over this period is -1.8 mm yr^{-1} for the combined effects of the 1924 and 1989 earthquakes.

Fig. 11(b) presents predicted relative sea level histories at the Macquarie Island tide gauge for the three earthquake scenarios. Linear rates of absolute sea level rise of 1.2 and 2.0 mm yr^{-1} combined with the deformation predictions of scenarios 1 and 2, respectively, yield excellent fits to the relative sea level time-series. Hence, we conclude that the high rate of relative sea level rise from our Macquarie Island tide gauge record is consistent with estimates of absolute sea level rise inferred in global studies (Church *et al.* 2004; Bindoff *et al.* 2007) once earthquake deformation has been taken into account. Similar fits to the GPS and relative sea level data sets could be achieved with a smaller 1924 earthquake, larger 1989 earthquake and greater absolute sea level rise. The lesser tectonic deformation of scenario 3 agrees with the lower bound of the short geodetic record but provides a poorer fit to the relative sea level data unless the rate of absolute sea level rise is as high as $\sim$3.2 mm yr^{-1} (Fig. 11b). Because scenario 2 reproduces the best estimate of GPS-observed subsidence, and the lower range of the GPS rate uncertainty and/or a greater 1989 earthquake imply greater absolute SLR, we conclude that the Macquarie Island relative sea level data are most compatible with an absolute rate of sea level rise that is in the upper half of the range of estimates for global mean rate for the twentieth century (Bindoff *et al.* 2007). This inference supports the regional sea level reconstructions for this area of the Southern Ocean that show marginally elevated rates of SLR with respect to the global average (Church *et al.* 2004).

As our modelling of post-seismic earthquake deformation is constrained only by the vertical GPS and relative sea level data, the predicted horizontal deformation from the earthquake scenarios in the period prior to the 2004.98 earthquake serve as an additional validation of the compatibility of the post-seismic modelling and geodetic observables. Figs 12(a) and (b) show the modelled time-series for the horizontal components corresponding to the predicted vertical deformation scenarios of Fig. 11(a). The observed tectonic velocity at MAC1 (on the Pacific Plate) relative to the stable Pacific Plate as defined by geodetic observations from the plate interior (Altamimi *et al.* 2007) in the 2000–2004.98 period of the T&W GPS time-series is 21° more convergent than the predicted motion of the stable Australian Plate in the same reference frame (Fig. 12c). In this time interval, the model predictions of post-seismic rate are consistent between the three scenarios, with a range of 0.2 mm yr^{-1} in East and 0.4 mm yr^{-1} in North. Subtracting the predicted post-seismic deformation rate of scenario 2 from the observed geodetic velocity prior to the 2004 earthquake yields a velocity vector parallel to the predicted motion across the plate boundary (Fig. 12c). In addition, the azimuth of predicted motion of the Macquarie Plate (Cande & Stock 2004) is $<2°$ from the Australian Plate prediction shown in Fig. 12(c). Although we do not have sufficient information on inter-seismic strain accumulation along this portion of the Australia–Pacific Plate boundary to use the horizontal predictions to refine the twentieth century earthquake sources, the agreement of Fig. 12(c) corroborates the validity of the post-seismic deformation modelling.

The uncertainties in the seismological observations, fault geometries, viscoelastic structure and absolute sea level change make such modelled scenarios non-unique. Therefore, we interpret the

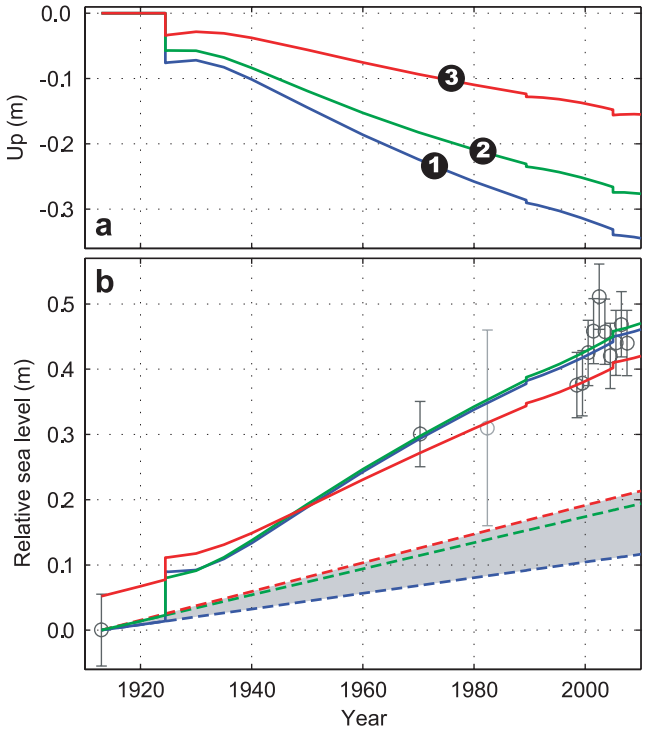

Figure 11. (a) Modelled cumulative vertical deformation time-series (scenarios 1, 2 and 3) at Macquarie Island incorporating coseismic and post-seismic deformation from great earthquakes in 1924, 1989 and 2004. Pre-2004 earthquake subsidence rates for scenarios 1, 2 and 3 match the high, best estimate and low ends of the GPS estimated rate and uncertainty, respectively. (b) Observed relative sea level (RSL) data (black circles with error bars as per Figure 5) with predicted relative sea level (blue, green and red solid lines) generated using deformation scenarios 1, 2 and 3 (same colours as top panel), fitted to RSL data and implying a linear change to absolute sea level (ASL) defined by the dashed lines. The dashed blue and green lines represent rises in ASL of +1.2 and +2.0 mm/yr, respectively, as best fit by the observed RSL data and scenario 1 (blue) and scenario 2 (green) deformation time-series. A rise of +2.2 mm/yr in ASL (dashed green line) is inferred from the less optimal fit of the observed RSL data and scenario 3 (solid red line, shifted to best fit RSL observed data, constrained at the upper bound of the 1912 estimate). The shaded grey region is indicative of the IPCC absolute global MSL trend and its uncertainty ($+1.7 \pm 0.5$ mm/yr) over the 20th century (Bindoff *et al.* 2007).

relatively good fit of the sea level and tectonic scenarios to the relative sea level data of Fig. 11(b) as indicative of a range of the most likely twentieth century tectonic and sea level histories for Macquarie Island, given the available constraints.

5 DISCUSSION AND CONCLUSION

This study illustrates the complexity of studying sea level rise in a plate–boundary setting where seismic deformation from multiple fault segments of a deforming region may contribute to the vertical motion of a tide gauge anchored to land. Given the long timescale and rate of the vertical post-seismic deformation derived for the 1924 earthquake, we infer that Macquarie Island shows the potential for great earthquakes that occurred prior to the instrumented period to cause modern rates of vertical deformation at the sub-mm yr^{-1} to mm yr^{-1} level. The large spatial extent of deformation from great earthquakes, particularly during the post-seismic phase, also has important implications for understanding the vertical stability of crust within thousands of kilometres of tectonic zones capable of generating great earthquakes, such as the MRC. Studies of sea level rise vulnerability for low-lying areas in tectonically active regions should consider the potential effects of relatively distant earthquakes in addition to near-field seismic sources.

The magnitude of ongoing deformation we observe due to post-seismic viscoelastic relaxation 80 yr after the northern Hjort Trench earthquake suggests that long-term post-seismic deformation may be a more ubiquitous component of plate boundary crustal velocity fields than widely appreciated. The similar surface deformation effects of post-seismic deformation and inter-seismic locking make it difficult to unambiguously separate the two processes in many settings. For example, Pollitz *et al.* (2008b) inferred that a significant portion of the contemporary crustal velocity in the western United States is due to ongoing post-seismic relaxation from the largest known earthquakes that occurred there in the past three centuries. However, they noted that purely elastic block modelling can achieve a similar fit to the observed horizontal GPS velocities in the same region. There are other examples in which decadal to centennial-duration post-seismic transient deformation is clear. Ongoing post-seismic deformation is required to match both vertical and horizontal post-seismic geodetic observations from the great Chile and Alaska earthquakes of 1960 and 1964 (e.g. Hu *et al.* 2004; Suito & Freymuller 2009). In the case of the Chile earthquake, a modelling study predicts that transient horizontal post-seismic deformation will be detectable in the near field for more than 300 yr following the earthquake (Lorenzo-Martin *et al.* 2006). Long-term viscoelastic deformation has been inferred for smaller crustal earthquakes as well. Observations of anomalous uplift rates (2–3 mm yr^{-1}) and horizontal contraction in the vicinity of central Nevada M_w 7 earthquakes that occurred 1915–1954 support the idea that the relaxation timescales for significant post-seismic deformation are long in comparison to the duration of modern geodetic measurements (Gourmelen & Amelung 2005). A global modelling study suggests that coseismic and post-seismic deformation from earthquakes in the instrumental record affect estimates of relative sea level rise at the global tide gauge network at the ~0.2 mm yr^{-1} level, and at much higher levels for regions in the near field of the largest earthquakes (Melini & Piersanti 2006).

The oceanic setting of Macquarie Island provides a relatively unique opportunity to interrogate the post-seismic response of oceanic lithosphere and mantle outside of the subduction zone setting. An important implication of our study is the support for a low-viscosity asthenosphere bounded relatively sharply by stronger upper mantle material both above and below, consistent with plate tectonic modelling and some GIA studies (Paulson & Richards 2009). Our inferred asthenospheric viscosity of 3×10^{19} Pa s is considerably higher than the best fitting value of 5×10^{17} Pa s from the regional oceanic seismicity study of Pollitz *et al.* (1998). However, Pollitz *et al.* (2006) suggested that this low value may represent the transient viscosity in a Burgers body rheology that has a steady-state viscosity of 1×10^{19} Pa s, which controls behaviour over longer timescales. Tectonic and post-glacial viscoelastic deformation at subduction zones partially reflects the rheology of oceanic asthenosphere, although it is complicated by 3-D heterogeneity including slabs and a hydrated continental mantle wedge. Subduction zone studies that explicitly address the viscosity of the oceanic asthenosphere infer steady state viscosities of 10^{18}–10^{20} Pa s (e.g. Hu *et al.* 2004; Pollitz *et al.* 2008a; James *et al.* 2009). Bürgmann & Dresen (2008) reviewed values of upper mantle viscosity inferred from geodetic studies, and our estimate lies at the high end of the range of viscosities from post-seismic studies in continental plate boundary settings, but considerably lower than the 10^{20}–10^{21} Pa s

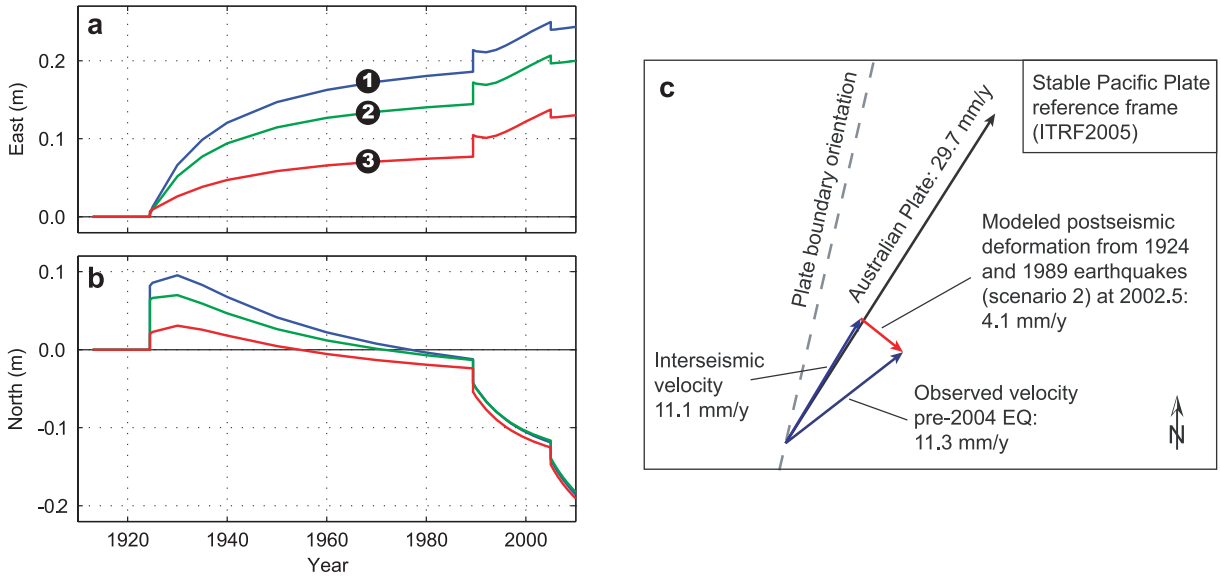

Figure 12. Modelled cumulative horizontal deformation time-series for (a) east and (b) north components from the three earthquake scenarios of Fig. 11. (c) Observed and modelled tectonic velocities at Macquarie Island. Removing the modelled post-seismic deformation rate from the 1924 and 1989 earthquakes (left panels) for the pre-2004 earthquake period of the GPS record makes the observed inter-seismic velocity at MAC1 parallel to the predicted Australia-Pacific relative motion, and supports the validity of the post-seismic modelling.

values from postglacial isostatic adjustment in cratonic settings. The intermediate viscosity for the oceanic upper mantle investigated in our study seems reasonable as the asthenosphere is likely not anomalously hot or hydrated like many of the plate boundary examples, nor is it as cold and dry as the upper mantle below cratons (Bürgmann & Dresen, 2008).

The greater sensitivity of the vertical component of post-seismic deformation to this aspect of the viscoelastic layering of the Earth (Pollitz 1997; Hearn 2003) makes estimates of vertical deformation from GNSS observations and relative sea level an important complement to horizontal geodetic measurements. If there are major viscosity contrasts at both the upper and lower limits of the asthenosphere, the enhanced rates and duration of the vertical deformation induced by viscoelastic relaxation following large earthquakes should be readily observable by modern geodetic techniques over relatively long time periods. Such observations, coupled with more accurate estimates of the crustal and upper mantle structure than are currently available for the MRC region, will greatly enhance our ability to infer rheologic properties of the outer Earth.

Although the twentieth century vertical motion at Macquarie Island is well described by only coseismic and post-seismic deformation from recent earthquakes, further work is needed to understand the full seismic cycle for this obliquely convergent oceanic plate boundary. Inter-seismic deformation along the Macquarie segment clearly affects the horizontal velocity observed at MAC1 (Fig. 12c), although the vertical component of such deformation is unclear. Massell *et al.* (2000) inferred that near Macquarie Island the MRC is bounded by oppositely verging thrust faults, with a major strike-slip fault running down the axis of the ridge. Assuming reasonable dips for the ridge-bounding thrusts, these faults likely intersect the central strike-slip zone and one another at depths of 10–40 km. In addition, the gravity signature along this segment of the MRC is not consistent with either of the thrusts accommodating lithospheric-scale displacement (Meckel *et al.* 2003). In light of these observations, we favour an interpretation that the thrusts, which may accommodate the 10 mm yr^{-1} boundary-normal component of Australia-Pacific motion (Fig. 12c), are less likely to be linked to a lithospheric-scale shear zone that would drive vertical inter-seismic deformation. We feel the central strike-slip structure, which would accommodate the 28 mm yr^{-1} of boundary-parallel deformation in a slip-partitioned system, most likely dominates the inter-seismic deformation, with relatively little vertical surface displacement. Future work that better characterizes the structural architecture of the MRC and contemporary measurements of the motion of the entirely submarine, inferred Macquarie Plate (Cande & Stock 2004) would greatly improve our understanding of tectonic processes along the MRC.

The strongest piece of evidence requiring the presence of a rheologically distinct, ∼140-km-thick asthenosphere below the MRC area comes from the significant change in uplift rate observed in the Macquarie Island MAC1 GPS record following the 2004.9771 earthquake. This significant rate change is not clearly observed in the coordinate time-series from other non-homogeneously reprocessed and typically more noisy global solutions (Fig. 6). Of interest here is the occurrence of the M_w 9.2 Sumatra-Andaman earthquake only days after the great Macquarie earthquake of 2004. Modelling of the coseismic deformation from the Sumatra event suggests mm-level static deformation occurred over the entire surface of the earth (Kreemer *et al.* 2006). As per Tregoning & Watson (2009), we selected appropriate sites located in regions of low predicted deformation to realize the terrestrial reference frame. The pervasive nature of the deformation does however highlight the challenge of maintaining a terrestrial reference frame capable of underpinning studies such as this one. This issue is further evidenced by the coseismic and post-seismic displacement following the Macquarie earthquake of 2004 at historically 'core' sites within the ITRF, including the IGS site HOB2, and the International VLBI Service for Geodesy and Astrometry (IVS) site HOBART26, both located in Tasmania, SE Australia (Fig. 7).

The rate of absolute sea level change inferred at the Macquarie Island tide gauge over the twentieth century is at the upper bound of the global average, with the most plausible estimate at the 2.0 ± 0.8 mm yr^{-1} level. With future refinement in the reference frame, and as the time-series of both GPS and sea level measurements

lengthen at Macquarie Island and other sites in the region, our inferences of the nature of the deformation will strengthen as will our ability to accurately infer the rheology underlying the current tectonic evolution of the Island. This further highlights the value of historical and recent observations of sea level, as well as space geodetic estimates of surface deformation, particularly in regions of such oceanographic and geological interest.

ACKNOWLEDGMENTS

The authors thank L. Wallace and P. Woodworth for their constructive reviews of this manuscript. This project was supported under the Australian Research Council's Discovery Projects funding scheme (DP0877381). The Australian Antarctic Division and expeditioners at the Macquarie Island station are thanked for their ongoing assistance with the operation and maintenance of the tide gauge. The authors thank the Mitchell library for assistance with AAE data and the National Tidal Centre for the provision of their digitised AAE tidal record. The authors thank Fred Pollitz for making his program VISCO1D freely available. Geoscience Australia and the International GNSS Service (IGS) are thanked for making the raw GPS data (including MAC1) used in this study publically available. The authors acknowledge the New Zealand GeoNet project and its sponsors EQC, GNS Science and LINZ, for providing the New Zealand raw GPS data that was processed as part of this study. Some of the figures were made with the Generic Mapping Tools software (Wessel & Smith, 1991).

REFERENCES

Abe, K., 1981. Magnitudes of large shallow earthquakes from 1904 to 1980, *Phys. Earth planet. Inter.,* **27,** 72–92.

Adamson, D.A., Selkirk, P.M., Price, D.M., Ward, N. & Selkirk, J.M., 1996. Pleistocene uplift and palaeoenvironments of Macquarie Island: evidence from palaeobeaches and sedimentary deposits, *Papers Proc., R. Soc. Tasmania,* **130**(2), 25–32.

Altamimi, Z., Sillard, P. & Boucher, C. 2002. ITRF2000: a new release of the International Terrestrial Reference Frame for earth science applications, *J. geophys. Res.,* **107**(B10), 2214, doi:10.1029/2001JB000561.

Altamimi, Z., Collilieux, X., Legrand, J., Garayt, B. & Boucher, C. 2007. ITRF2005: a new release of the International Terrestrial Reference Frame based on time series of station positions and Earth Orientation Parameters, *J. geophys. Res.,* **112,** B09401, doi:10.1029/2007JB004949.

Anderson, H.J. & Zhang, J.J., 1991. Long-period seismic radiation from the May 23, 1989 Macquarie Ridge earthquake: evidence for coseismic slip in the mantle? *J. geophys. Res.,* **96,** 19 853–19 863.

Argus, D.F., 2007. Defining the translational velocity of the reference frame of Earth, *Geophys. J. Int.,* **169,** 830–838.

Argus, D.F., Gordon, R.G., Heflin, M.B., Ma, C., Eanes, R.J., Willis, P., Peltier, W.R. & Owen, S.E., 2010. The angular velocities of the plates and the velocity of Earth's centre from space geodesy, *Geophys. J. Int.,* **180,** 913–960.

Bindoff, N.L. *et al*. 2007. Observations: oceanic climate change and sea level, in *Climate Change 2007: The Physical Science Basis—Contribution of Working Group I to the Fourth Assessment Report of the Intergovernmental Panel on Climate Change,* pp. 385–432, ed. Solomon, S. *et al*., Cambridge University Press, New York.

Braunmiller, J. & Nabelek, J., 1990. Rupture process of the Macquarie Ridge earthquake of May 23, 1989, *Geophys. Res. Lett.,* **17,** 1017–1020.

Brune, J.N. & King, C.Y., 1967. Excitation of mantle Rayleigh waves of period 100 seconds as a function of magnitude, *Bull. seism. Soc. Am.,* **57,** 1355–1365.

Bürgmann, R. & Dresen, G., 2008. Rheology of the lower crust and upper mantle: evidence from rock mechanics, geodesy, and field observations, *Ann. Rev. Earth planet. Sci.,* **36,** 531–567.

Cande, S.C. & Stock, J.M., 2004. Pacific-Antarctic-Australia motion and the formation of the Macquarie Plate, *Geophys. J. Int.,* **157,** 399–414.

Church, J.A., White, N.J., Coleman, R., Lambeck, K. & Mitrovica, J.X., 2004. Estimates of the regional distribution of sea level rise over the 1950–2000 period, *J. Clim.,* **17**(13), 2609–2625.

Corcoran, J., 1982. Macquarie Island Sea Level Connection, Division of National Mapping, Field book NM 19366.

Das, S., 1992. Reactivation of an oceanic fracture by the Macquarie Ridge earthquake of 1989, *Nature,* **357,** 150–153.

Das, S., 1993. The Macquarie Ridge earthquake of 1989, *Geophys. J. Int.,* **115,** 778–798.

Davis, J.L. & Mitrovica, J.X., 1996. Glacial isostatic adjustment and the anomalous tide gauge record of eastern North America, *Nature,* **379**(6563), 331–333.

Doodson, A.T., 1939. *Oceanography Part 2: Tidal Observations, Scientific Reports from the Australasian Antarctic Expedition 1911–1914,* pp. 61–85, Series A(2), Australian Government Printers, Sydney, Australia.

Dow, J.M., Neilan, R.E. & Gendt, G., 2005. The international GPS service: celebrating the 10th anniversary and looking to the next decade, *Adv. Space Res.,* **36**(3), 320–326.

Duncan, R.A. & Varne, R., 1988. The age and distribution of igneous rocks on Macquarie Island, *Papers Proc., R. Soc. Tasmania,* **122**(1), 45–50.

Ekström, G. & Dziewonski, A.M., 1988. Evidence of bias in estimations of earthquake size, *Nature,* **332,** 319–323.

Ekström, G. & Romanowicz, B., 1990. The 23 May 1989 Macquarie Ridge earthquake: a very broad-band analysis, *Geophys. Res. Lett.,* **17,** 993–996.

Emery, K.O. & Aubrey, D.G., 1991. *Sea Levels, Land Levels, and Tide Gauges,* Springer-Verlag, New York.

Frohlich, C., Coffin, M.F., Massell, C., Mann, P., Schuur, C.L., Davis, S.D., Jones, T. & Karner, G., 1997. Constraints on Macquarie Ridge tectonics provided by Harvard focal mechanisms and teleseismic earthquake locations, *J. geophys. Res.,* **102**(B3), 5029–5041.

Geoscience Australia, 2008. Geodetic Connections to the Macquarie Island Tide Gauge Benchmarks, Geoscience Australia, Canberra, Australia, http://www.ga.gov.au/geodesy/antarc/antgauge.jsp.

Gourmelen, N. & Amelung, F., 2005. Postseismic mantle relaxation in the Central Nevada Seismic Belt, *Science,* **310,** 1473–1476.

Gutenberg, B. & Richter, C.F., 1949. *Seismicity of the Earth and Associated Phenomena,* p. 273, Princeton University Press, Princeton.

Hayes, G.P., Furlong, K.P. & Ammon, C.J., 2009. Intraplate deformation adjacent to the Macquarie Ridge south of New Zealand-The tectonic evolution of a complex plate boundary, *Tectonophysics,* **463,** 1–14.

Hearn, E.H., 2003. What can GPS data tell us about the dynamics of postseismic deformation?, *Geophys. J. Int.,* **155,** 753–777.

Herring, T.A., King, R.W. & McClusky, S.C., 2008. *Introduction to GAMIT/GLOBK,* Massachusett Institute of Technology, Cambridge.

Hu, Y., Wang, K., He, J., Klotz, J. & Khazaradze, G. 2004. Three-dimensional viscoelastic finite element model for postseismic deformation of the great 1960 Chile earthquake, *J. Geophys. Res.,* **109,** B12403.

Hunter, J., Coleman, R. & Pugh, D., 2003. The sea level at Port Arthur, Tasmania, from 1841 to the present, *Geophys. Res. Lett.,* **30**(7), 1401, doi:10.1029/2002GL016813.

James, T.S., Gowan, E.J., Wada, I., & Wang, K., 2009. Viscosity of the asthenosphere from glacial isostatic adjustment and subduction dynamics at the northern Cascadia subduction zone, British Columbia, Canada, *J. geophys. Res.,* **114,** B04405.

Jevrejeva, S., Grinsted, A., Moore, J.C. & Holgate, S., 2006. Nonlinear trends and multiyear cycles in sea level records, *J. geophys. Res.,* **111,** C09012, doi:10.1029/2005JC003229.

Kawakatsu, H., Kumar, P., Takei, Y., Shinohara, M., Kanazawa, T., Araki, E. & Suyehiro, K., 2009. Seismic evidence for sharp lithosphere-asthenosphere boundaries of oceanic plates, *Science,* **324,** 499–502.

Keller, W.R., 2004. Cenozoic plate tectonic reconstructions and plate boundary processes in the Southwest Pacific, *PhD thesis*. California Institute of Technology, Pasadena, California.

Kreemer, C., Blewitt, G., Hammond, W.C. & Plag, H.P., 2006. Global deformation from the great 2004 Sumatra-Andaman Earthquake observed by

GPS: implications for rupture process and global reference frame, *Earth Planets Space,* **58,** 141–148.

Lebrun, J.F., Lamarche, G. & Collot, J.Y., 2003. Subduction initiation at a strike-slip plate boundary: the Cenozoic Pacific-Australian plate boundary, south of New Zealand, *J. geophys. Res.,* **108,** 2453.

Leuliette, E.W., Nerem, R.S. and Mitchum, G.T. 2004. Calibration of TOPEX/POSEIDON and Jason altimeter data to construct a continuous record of mean sea level change, *Mar. Geod.,* **27**, 79–94.

Lorenzo-Martin, F., Roth, F. & Wang, R.J., 2006. Inversion for rheological parameters from post-seismic surface deformation associated with the 1960 Valdivia earthquake, Chile, *Geophys. J. Int.,* **164,** 75–87.

Massell, C. *et al*. 2000. Neotectonics of the Macquarie Ridge Complex, Australia-Pacific plate boundary, *J. geophys. Res.,* **105,** 13 457–13 480.

Maul, G.A. & Martin, D.M., 1993. Sea level rise at Key West, Florida, 1846–1992: America's longest instrument record? *Geophys. Res. Lett.,* **20**(18), 1955–1958.

McCue, K.F., 1971. *Macquarie Island Geophysical Observatory, Annual Report 1969*, Department of National Development, Bureau of Mineral Resources, Geology and Geophysics, Record No. 1971/13.

McKenzie, D., Jackson, J. & Priestley, K., 2005. Thermal structure of oceanic and continental lithosphere, *Earth planet. Sci. Lett.,* **233,** 337–349.

Meckel, T.A., Coffin, M.F., Mosher, S., Symonds, P., Bernardel, G. & Mann, P., 2003. Underthrusting at the Hjort Trench, Australian-Pacific plate boundary: Incipient subduction?, *Geochem. Geophys. Geosyst.,* **4,** 1099, doi:10.1029/2002GC000498.

Meckel, T.A., Mann, P., Mosher, S. & Coffin, M.F., 2005. Influence of cumulative convergence on lithospheric thrust fault development and topography along the Australian-Pacific plate boundary south of New Zealand, *Geochem. Geophys. Geosyst.,* **6,** Q09010.

Melini, D. & Piersanti, A., 2006. Impact of global seismicity on sea level change assessment, *J. geophys. Res.,* **111,** B03406.

Milne, G.A., Davis, J.L., Mitrovica, J.X., Scherneck, H.G., Johansson, J.M., Vermeer, M. & Koivula, H., 2001. Space-geodetic constraints on glacial isostatic adjustment in Fennoscandia, *Science,* **291**(5512), 2381–2385.

Moore, M.A., Anderson, H.J. & Pearson, C., 2000. Seismic and geodetic constraints on plate boundary deformation across the northern Macquarie Ridge and southern South Island of New Zealand, *Geophys. J. Int.,* **143,** 847–880.

National Tidal Centre, 2005. The Australian baseline sea level monitoring project: Annual Sea Level Data Summary Report, July 2004–June 2005, http://www.bom.gov.au/ntc/IDO60202/IDO60202.2005.pdf.

Okada, Y., 1992. Internal deformation due to shear and tensile faults in a half-space, *Bull. seism. Soc. Am.,* **82,** 1018–1040.

Pacheco, J.F. & Sykes, L.R., 1992. Seismic moment catalog of large shallow earthquakes, 1900 to 1989, *Bull. seism. Soc. Am.,* **82,** 1306–1349.

Paulson, A. & Richards, M.A., 2009. On the resolution of radial viscosity structure in modelling long-wavelength postglacial rebound data. *Geophys. J. Int.,* **179,** 1516–1526.

Pawlowicz, R., Beardsley, B. & Lentz, S., 2002. Classical tidal harmonic analysis including error estimates in MATLAB using T_TIDE, *Comput. Geosci.,* **28**(8), 929–937.

Peltier, W.R., 2004. Global glacial isostasy and the surface of the Ice-Age Earth: The ICE-5G (VM2) model and GRACE, *Ann. Rev. Earth planet. Sci.,* **32,** 111–149.

Pollitz, F.F., 1997. Gravitational viscoelastic postseismic relaxation on a layered spherical Earth, *J. geophys. Res.,* **102,** 17 921–17 941.

Pollitz, F.F., Bürgmann, R. & Romanowicz, B., 1998. Viscosity of oceanic asthenosphere inferred from remote triggering of earthquakes, *Science,* **280,** 1245–1249.

Pollitz, F.F., Bürgmann, R. & Banerjee, P., 2006. Post-seismic relaxation following the great 2004 Sumatra-Andaman earthquake on a compressible self-gravitating Earth, *Geophys. J. Int.,* **167,** 397–420.

Pollitz, F.F., Banerjee, P., Grijalva, K., Nagarajan, B. & Bürgmann, R., 2008a. Effect of 3-D viscoelastic structure on post-seismic relaxation from the 2004 M = 9.2 Sumatra earthquake, *Geophys. J. Int.,* **173,** 189–204.

Pollitz, F.F., McCrory, P., Svarc, J. & Murray, J., 2008b. Dislocation models of interseismic deformation in the western United States, *J. geophys. Res.,* **113,** B04413.

Pugh, D., 1987. *Tides, Surges and Mean Sea Level: A Handbook for Engineers and Scientists,* John Wiley and Sons, Chichester.

Ruff, L.J., Given, J.W., Sanders, C.O. & Sperber, C.M., 1989. Large earthquakes in the Macquarie Ridge complex: transitional tectonics and subduction initiation, *Pure appl. Geophys.,* **129,** 71–129.

Satake, K. & Kanamori, H., 1990. Fault parameters and tsunami excitation of the May 23, 1989, Macquarie Ridge earthquake, *Geophys. Res. Lett.,* **17,** 997–1000.

Shinohara, M. *et al*. 2008. Upper mantle and crustal seismic structure beneath the Northwestern Pacific Basin using a seafloor borehole broadband seismometer and ocean bottom seismometers, *Phys. Earth planet. Inter.,* **170,** 95–106.

Sokolov, S. & Rintoul, S.R., 2007. Multiple jets of the antarctic circumpolar current South of Australia, *J. Phys. Oceanogr.,* **37**(5), 1394–1412.

Suito, H. & Freymueller, J.T., 2009. A viscoelastic and afterslip postseismic deformation model for the 1964 Alaska earthquake, *J. geophys. Res.,* **114,** B11404.

Testut, L., Wöppelmann, G., Simon, B. & Techine, P., 2006. The sea level at Port-aux-Francais, Kerguelen Island, from 1949 to the present, *Ocean Dyn.,* **56**(5–6), 464–472.

Tichelaar, B.W. & Ruff, L.J., 1990. Rupture process and stress-drop of the great 1989 Macquarie Ridge earthquake, *Geophys. Res. Lett.,* **17,** 1001–1004.

Tregoning, P. & Watson, C.S., 2009. Atmospheric effects and spurious signals in GPS analysis, *J. geophys. Res.,* **114,** B09403, doi:10.1029/2009JB006344.

Valenzuela, R.W. & Wysession, M.E., 1993. Intraplate earthquakes in the southwest Pacific Ocean basin and the seismotectonics of the southern Tasman Sea, *Geophys. Res. Lett.,* **20,** 2467–2470.

Velasco, A.A., Ammon, C.J. & Lay, T., 1995. Source time function complexity of the great 1989 Macquarie Ridge earthquake, *J. geophys. Res.,* **100,** 3989–4009.

Watson, C., Coleman, R. & Handsworth, R., 2008. Coastal Tide Gauge Calibration: a case study at Macquarie Island using GPS Buoy techniques, *J. Coastal Res.,* **24**(4), doi: 10.2112/2107-0844.

Wertz, K.L., 2003. From seafloor spreading to uplift: the structural and geochemical evolution of Macquarie Island on the Australian-Pacific plate boundary, *PhD thesis*. The University of Texas, Austin.

Wessel, P. & Smith, W.H.F. 1991. Free software helps map and display data, *EOS, Trans. Am. geophys. Un*., **72,** 441.

Williams, S.D.P., 2008. CATS: GPS coordinate time series analysis software, *GPS Solut.,* **12**(2), 147–153.

Woodworth, P.L., 1999. High waters at Liverpool since 1768: the UK's longest sea level record, *Geophys. Res. Lett.,* **26**(11), 1589–1592.

Woodworth, P.L. & Player, R., 2003. The Permanent Service for Mean Sea Level: An update to the 21st century, *J. Coastal Res.,* **19,** 287–295.

Woodworth, P.L., Pugh, D.T. & Bingley, R.M., 2010. Long term and recent changes in sea level in the Falkland Islands, *J. geophys. Res,* in press.

Wöppelmann, G., Pouvreau, N. & Simon, B., 2006. Brest sea level record: a time series construction back to the early eighteenth century, *Ocean Dyn.,* **56**(5–6), 487–497.

Wöppelmann G., Letetrel, C., Santamaria, A., Bouin, M-N., Collilieux, X., Altamimi, Z., Williams, S.D.P. & Martin Miguez B., 2009. Rates of sea-level change over the past century in a geocentric reference frame. *Geophys. Res. Lett.,* **36,** L12607, doi:10.1029/2008GL038720.